LETTERS

Structural basis for selective recognition of ESCRT-III by the AAA ATPase Vps4

Takayuki Obita[1], Suraj Saksena[2], Sara Ghazi-Tabatabai[1], David J. Gill[1], Olga Perisic[1], Scott D. Emr[2] & Roger L. Williams[1]

The AAA+ ATPases are essential for various activities such as membrane trafficking, organelle biogenesis, DNA replication, intracellular locomotion, cytoskeletal remodelling, protein folding and proteolysis[1]. The AAA ATPase Vps4, which is central to endosomal traffic to lysosomes[2,3], retroviral budding[4] and cytokinesis[5], dissociates ESCRT complexes (the endosomal sorting complexes required for transport) from membranes[6–15]. Here we show that, of the six ESCRT-III-related subunits in yeast, only Vps2 and Did2 bind the MIT (microtubule interacting and transport) domain of Vps4, and that the carboxy-terminal 30 residues of the subunits are both necessary and sufficient for interaction. We determined the crystal structure of the Vps2 C terminus in a complex with the Vps4 MIT domain, explaining the basis for selective ESCRT-III recognition. MIT helices α2 and α3 recognize a (D/E)xxLxxRLxxL(K/R) motif, and mutations within this motif cause sorting defects in yeast. Our crystal structure of the amino-terminal domain of an archaeal AAA ATPase of unknown function shows that it is closely related to the MIT domain of Vps4. The archaeal ATPase interacts with an archaeal ESCRT-III-like protein even though these organisms have no endomembrane system, suggesting that the Vps4/ESCRT-III partnership is a relic of a function that pre-dates the divergence of eukaryotes and Archaea.

The Vps4 AAA ATPase has a key function in the endocytic pathway for the degradation of membrane proteins, and it is recruited to endosomes by means of an N-terminal MIT domain[7,16]. On binding ATP, Vps4 assembles into an oligomer thought to consist of two stacked hexameric rings[7,17]. Proteins bound to the rings experience mechanical forces coupled to conformational changes that occur during catalysis.

Vps4 function is tightly linked to ESCRTs, the multiprotein complexes required for the sorting of endocytosed transmembrane proteins into intraluminal vesicles (ILVs) of morphologically distinctive endosomes known as multivesicular bodies (MVBs). Inward budding of the endosomal limiting membrane generates ILVs, and subsequent fusion of endosomes with lysosomes leads to the hydrolysis of ILVs and their cargo proteins. Vps4 deletion results in an accumulation of all ESCRTs on endosomes[2,3]. ESCRT-III subunits transiently recruit Vps4 to endosomes.

There are six families of ESCRT-III-like proteins[8,18], namely the Vps2, Vps20, Vps24, Snf7, Did2 and Vps60 subunits in yeast. ESCRT-III subunits have a basic N-terminal four-helical core[19] and an acidic C-terminal region. They can homodimerize and heterodimerize through their N-terminal regions, but they also have a metastable, monomeric, closed form in which the C-terminal region blocks heterodimerization[20,21]. The C-terminal region of some ESCRT-III subunits can also recruit MIT-domain-containing proteins such as Vps4 and the deubiquitinase AMSH[17,21–23]. Several ESCRT-III subunits can interact directly with membranes[18,20,24,25]; combined with their ability to homodimerize and heterodimerize, this means that the ESCRT-III subunits can form lattices with great avidity for membranes. This may account for the requirement of an ATPase to disassemble such lattices efficiently (Supplementary Fig. 1).

Vps2 and Vps24 are required for the recruitment of Vps4 to endosomes[6,18]. Both full-length Vps2 and C-terminal constructs bind directly to the Vps4 MIT domain (Fig. 1a–c). A construct consisting only of residues 183–232 binds the MIT domain with a K_d of 28 μM (Fig. 1d), and we determined the 2.0 Å resolution structure of it in a complex with the MIT domain of Vps4 (Supplementary Table 1).

The MIT domain consists of three antiparallel helices arranged in a slightly asymmetric fashion (Fig. 1e, g). The MIT-interacting region of Vps2 has three short helical segments, αA, αB and αC (Fig. 1e). Helices αA and αB are single-turn helices joined through a turn at Pro 195 and flanked by extended structure. The last helix, αC, is the longest and is separated from helix αB by a disordered region of ten residues.

Vps2 helix αC contacts MIT helices α2 and α3 and runs parallel with α3. Leu 64^{Vps4} and Glu 68^{Vps4} form key interactions with Arg 224^{Vps2} in the middle of αC (Fig. 1f, i). The mutation of analogous residues in the MIT domain of human Vps4A significantly decreased CHMP1B binding[15]. This central anchor is flanked by additional important hydrophobic interactions and salt links.

Although the crystal structure of the MIT domain of yeast Vps4 agrees closely with NMR structures of the MIT domains of human Vps4A (ref. 15) and Vps4B (ref. 26), our structure of the complex with Vps2 shows that the interaction with ESCRT-III differs from two models that were proposed on the basis of isolated MIT-domain structures. One model[26] proposed that an ESCRT-III subunit would slot into a shallow indentation between MIT helices α1 and α3, corresponding to the locations of Vps2 helices αA and αB in the Vps2–MIT complex. In contrast, another study proposed that an ESCRT-III helix interacts with MIT helix α3 to complete an overall tetratricopeptide repeat (TPR) fold, with the four MIT–ESCRT-III helices packed into a right-handed solenoid[15]. Our structure shows that Vps2 αC fits between MIT helices α2 and α3, but in an orientation opposite to what it would have in a TPR-like arrangement; that is, helix αC packs parallel with MIT helix α3 (Fig. 1e, g).

Six residues along one face of helix αC interact with the MIT domain (Fig. 1f), burying 562 and 676 $Å^2$ of solvent-accessible surface on Vps4 and Vps2, respectively. Leu 221^{Vps2}, Leu 225^{Vps2}, Leu 228^{Vps2} and the hydrophobic portion of Arg 224^{Vps2} form hydrophobic interactions. Three αC residues participate in salt links with the MIT domain, one in the middle (Arg 224^{Vps2}:Glu 68^{Vps4}) and one on each end of αC (Asp 218^{Vps2}:Arg 57^{Vps4} and Lys 229^{Vps2}:Asp 38^{Vps4}). These six ESCRT-III residues define a (D/E)xxLxxRLxxL(K/R) MIT-interacting

[1]MRC Laboratory of Molecular Biology, Medical Research Council Centre, Cambridge CB2 0QH, UK. [2]Department of Molecular Biology and Genetics and Institute for Cell and Molecular Biology, Biotechnology Building, Cornell University, Ithaca, New York 14853, USA.

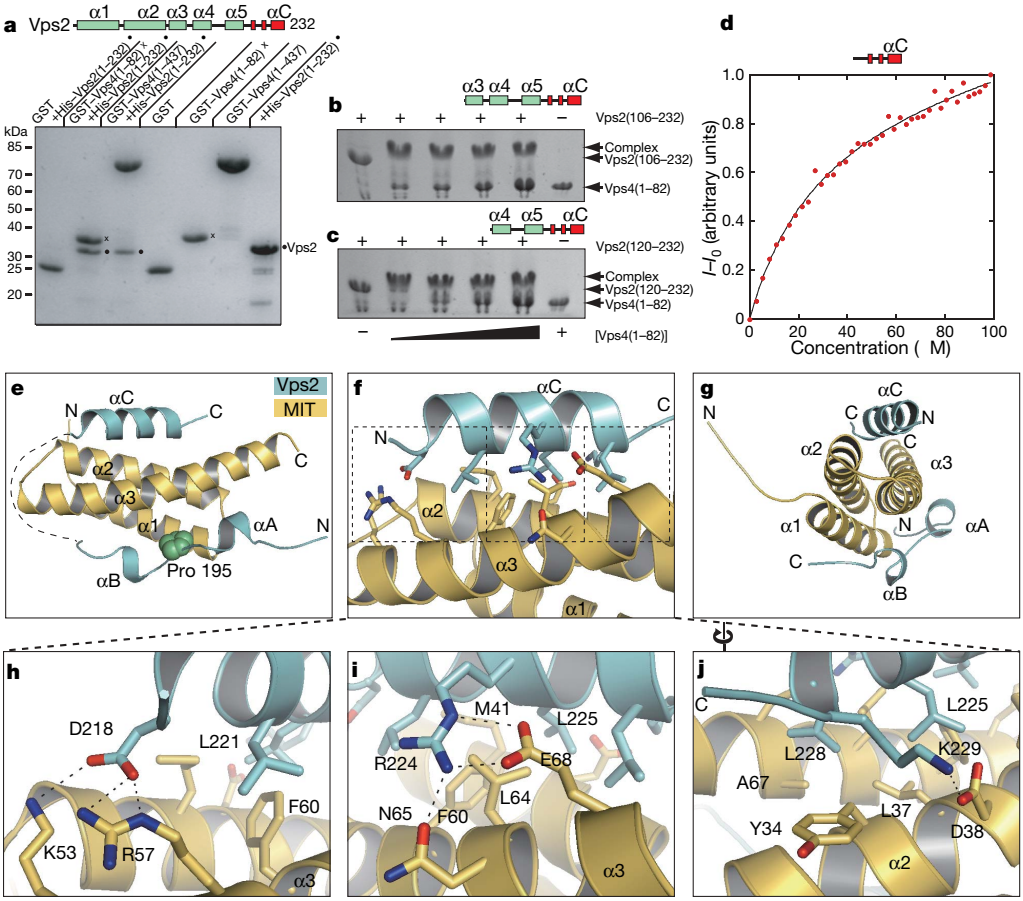

Figure 1 | Characterization of the Vps4–Vps2 complex. **a**, GST-tagged MIT domain of yeast Vps4 and full-length Vps4 interact with full-length Vps2. Coomassie-stained SDS–PAGE shows the material bound to the glutathione-Sepharose resin. **b**, **c**, Vps2 C-terminal constructs (residues 106–232 in **b** and residues 120–232 in **c**) also interact with an untagged MIT domain as detected by band-shift on native PAGE. **d**, Vps2 C-terminal region (residues 183–232) binds to the FlAsH-tagged Vps4 MIT domain with a K_d of 28 μM. **e**, Structure of the complex between Vps2 (cyan) and the Vps4 MIT domain (yellow). **f**, Interactions between Vps2 αC and MIT domain. **g**, The distinctive three-corners-of-a-square appearance of the three-helix MIT bundle. **h**–**j**, Enlarged central (**i**) and peripheral Vps2 helix αC specificity determinants (N-terminal and C-terminal regions are shown in **h** and **j**, respectively).

motif (MIM). We shall refer to these six residues as positions −2, −1, 0, +1, +2 and +3, with the anchoring Arg 224^{Vps2} defined as position 0 (Fig. 2a, b). Point mutations within the Vps2 MIM at positions −1, 0, +1, +2 and +3 eliminate MIT-domain binding *in vitro* (Fig. 2c). MIM residues can be divided into three pairs, a central pair and two peripheral pairs. Within each pair, a hydrophobic residue contributes to affinity and a polar residue contributes to both affinity and specificity of the interaction.

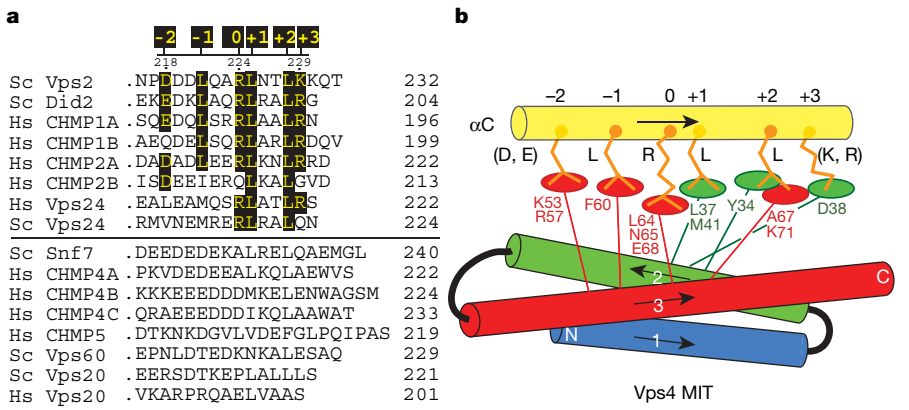

c

Mutant	Binding affinity (M)	*n*
Vps2(183–232)	28.0 ± 4.8	6
Vps2(154–232)	24.5 ± 4.6	3
Vps2(201–232)	29.7 ± 2.1	2
Vps2(208–232)	29.4 ± 1.9	3
Vps2(218–232)	26.8 ± 0.3	2
Vps2(183–232) L190D	32.5 ± 6.9	5
Vps2(183–232) E198R	20.0 ± 1.8	3
Vps2(183–232) T199D	28.1 ± 2.6	3
Vps2(183–232) L221D	No binding	
Vps2(183–232) R224D	No binding	
Vps2(183–232) L225D	No binding	
Vps2(183–232) L228D	No binding	
Vps2(183–232) K229D	No binding	

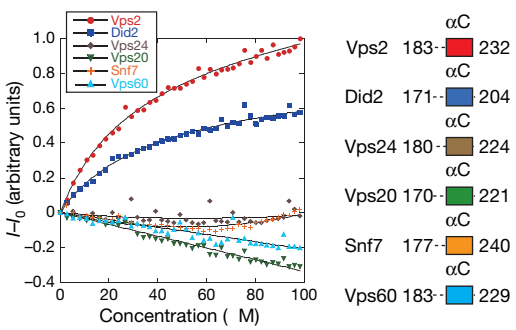

Figure 2 | A conserved MIT-interacting motif in ESCRT-III is critical for binding the Vps4 MIT domain. **a**, Alignment of the C-terminal regions of yeast (Sc) and human (Hs) ESCRT-III subunits. Vps2, Did2 and Vps24 homologues form a distinct group. Residues analogous to Vps2 αC residues contacting Vps4 MIT domain are highlighted. Snf7, Vps20 and Vps60 homologues are more divergent. **b**, Diagram of the ESCRT-III (D/E)xxLxxRLxxL(K/R) motif (yellow). **c**, Binding affinities of Vps2 mutants for MIT domain. Mutations in the MIM impair binding, and helix αC is sufficient for binding. Errors indicate s.d. **d**, Affinities of C-terminal regions from the six ESCRT-III subunits were determined by titration into FlAsH-tagged Vps4 MIT domains. Vps2 and Did2 bind with K_d values of 28 and 39 μM, respectively, and only they have MIMs. No other ESCRT-III binds at concentrations up to 100 μM.

Arg 224^{Vps2} uses both polar guanidinium and aliphatic portions of its side chain to anchor into a central, predominantly hydrophobic socket on the MIT domain made up of Met 41, Phe 60, Leu 64, Asn 65 and Glu 68 (Fig. 1i), forming a salt link with Glu 68^{Vps4}, a hydrogen bond with the Asn 65^{Vps4} side chain, and hydrophobic contacts with Leu 64^{Vps4}. The adjacent Leu 225^{Vps2} fills the bulk of the central, hydrophobic MIT-domain socket. The socket character is conserved between Vps4 MIT domains; however, one of the hydrogen-bonded partners for the central Arg varies (Asn 65 for yeast Vps4 and Asp for Vps4A and Vps4B). This conservation is consistent with the fact that mammalian orthologues are able to complement yeast Vps4 (ref. 27).

Amino-terminal residues of Vps2 αC (MIM positions −1 and −2) interact with MIT α3 (Fig. 1h). The hydrophobic residue at position −1 (Leu 221^{Vps2}) packs against Vps4 Phe 60. The acidic residue at position −2 (Asp 218^{Vps2}) forms salt links with MIT Lys 53^{Vps4} and Arg 57^{Vps4}. At the C-terminal end of helix αC, another pair of residues forms the third set of ESCRT-III–MIT interactions (Fig. 1j), involving primarily MIT helix α2. The hydrophobic residue at the +2 position (Leu 228^{Vps2}) packs against Vps4 Tyr 30, Tyr 34 and Leu 37 in helix α2 and against Ala 67 in helix α3. The +3 basic residue (Lys 229^{Vps2}) interacts with an acidic residue from Vps4 MIT helix α2 (Asp 38^{Vps4}).

Among yeast ESCRT-III-like subunits, only Vps2 and Did2 have the MIM motif (Fig. 2a). Consistent with this is our observation that the MIT domain of Vps4 binds only to Vps2 (K_d 28 μM) and Did2 (K_d 39 μM) (Fig. 2d). Searching the sequence database for MIM motifs identifies Vps2, Did2, CHMP1A and CHMP2A. CHMP1B has a single deviation from this motif, a Gln at position −2 (Gln 185), instead of an acidic residue, but it has a Glu immediately preceding it that may form a similar interaction. Indeed, CHMP1B binds human Vps4A MIT domain with a K_d of 20 μM (ref. 15). CHMP2B, which interacts very poorly with Vps4 (refs 10, 11), lacks the central Arg and has no peripheral basic residues. Yeast Vps24 lacks both the acidic residue at −2 and the basic residue at +3, and does not bind Vps4 (Fig. 2a). Human Vps24 (CHMP3) has a hydrophobic residue instead of an acidic residue at −2, and Met instead of Leu at position −1. These differences might weaken its interaction with Vps4 and explain why there have been conflicting reports about the interaction between Vps4 and human Vps24 (refs 10, 11, 13, 21).

To test whether MIMs have a role in sorting, we mutated motifs in both Vps2 and Did2. Single mutations of either Vps2 (R224D) or Did2 (R198D) or a double Did2 mutant, L199D/L202D, cause partial sorting defects, resulting in mislocalization of green fluorescent protein (GFP)–carboxypeptidase S (CPS) to the limiting membrane of the vacuole. In contrast, a double Vps2 mutant, L228D/K229D, causes a severe sorting defect manifested by a class E compartment (Fig. 3). These results show that MIM motifs are crucial for sorting in yeast.

Vps2 helices αA and αB contact the MIT domain, burying 659 and 723 Å^2 of solvent-accessible surface on Vps4 and Vps2, respectively. Pro 195, separating helices αA and αB, inserts into a conserved MIT pocket. One wall of this pocket is formed by a conserved intramolecular salt link between Asp 21 and Arg 66. However, we find that αA and αB have no influence on MIT binding (Fig. 2c), suggesting that their interactions are due to crystal packing. Consistent with this, there is no sequence similarity between Vps2 and Did2 in the region corresponding to αA and αB.

Other AAA ATPases such as spastin and spartin also have MIT domains, which might be important for their cellular localization[28]. To understand the role of MIT domains in restricting ATPase targets, we compared structural features in more distantly related ATPases. Towards this end, we determined the structure (Supplementary Table 2) of the MIT domain of an archaeal ATPase from *Sulfolobus solfataricus* (SSO0909), which has been annotated as a 'p60 katanin-like' ATPase. The MIT fold is closely conserved, with a Cα root mean squared deviation of only 1.8 Å between the yeast and archaeal MIT domains (Fig. 4). Most conserved features involve hydrophobic packing in the interior, but there is one key salt link, analogous to the Asp 21/Arg 66 link in yeast Vps4, that is universally conserved (Fig. 4a–d). All MIT domains appear as a four-helix bundle lacking one helix. In the archaeal and spartin MIT domains, the slot between helices α2 and α3 lacks specificity determinants important for MIM binding (Fig. 4c). The area analogous to the Vps4 socket that interacts with the central anchor region of the MIM has a basic residue in place of the Leu64^{Vps4} affinity determinant (Lys 65 in *S. solfataricus* ATPase and Arg 89 in spartin). This may reflect a binding surface that evolved to recognize a different target MIM. Structural similarity of archaeal and Vps4 MIT domains, together with the observation that Archaea have ESCRT-III-like subunits (see below), suggests that the archaeal ATPase is more Vps4-like than katanin-like.

All clades of eukaryotes have ESCRTs[29]. All Archaea that have a Vps4-like ATPase also have ESCRT-III-like homologues that form a closely related group (Supplementary Fig. 2), although they do not seem to have ESCRT-0, ESCRT-I or ESCRT-II. Moreover, one ESCRT-III-like subunit is always immediately adjacent to the gene for the Vps4-like ATPase (in *S. solfataricus*, the adjacent ESCRT-III-like subunit is SSO0910). The conserved tandem arrangement of these genes suggests that they might encode functional partners. Indeed, we find that a C-terminal region of SSO0910 binds directly to the archaeal Vps4-like ATPase MIT domain, and residues 164–207 of the ESCRT-III-like protein are both necessary and sufficient for

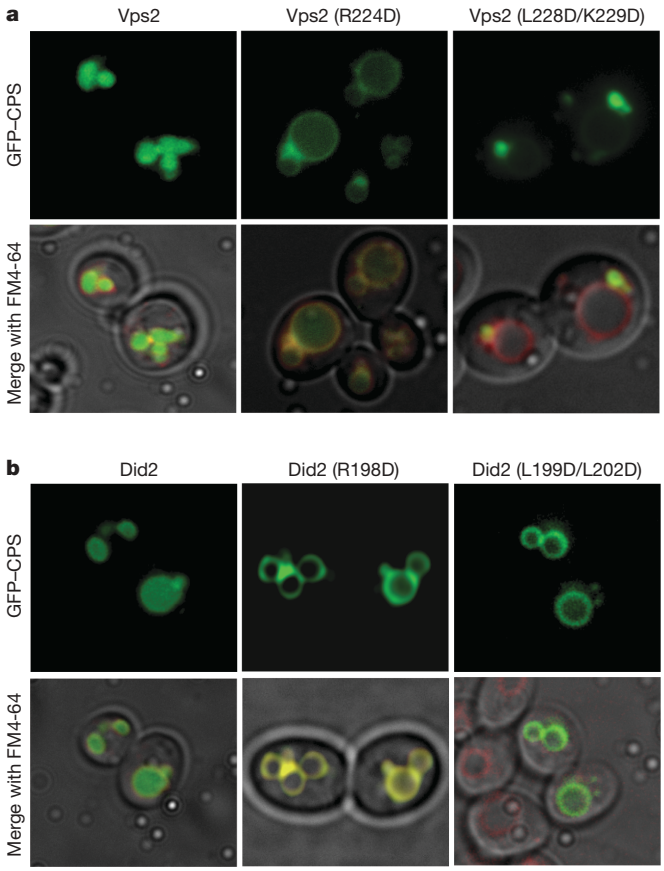

Figure 3 | MIT-interacting motifs in Vps2 and Did2 are important for function *in vivo*. **a**, In wild-type cells, GFP-tagged carboxypeptidase-S accumulates in the vacuolar lumen (FM4-64 preferentially labels the limiting membrane of the vacuole). A single mutation at position 0 of the Vps2 MIM (R224D) impairs sorting, and the GFP–CPS accumulates in the limiting membrane of the vacuole. A double mutation of the Vps2 MIM (L228D/K229D) causes GFP–CPS accumulation in a class E compartment. **b**, Both a single mutation at position 0 of the Did2 MIM (R198D) and a double mutation (L199D/L202D) impair sorting of GFP–CPS, which accumulates in the limiting membrane of the vacuole.

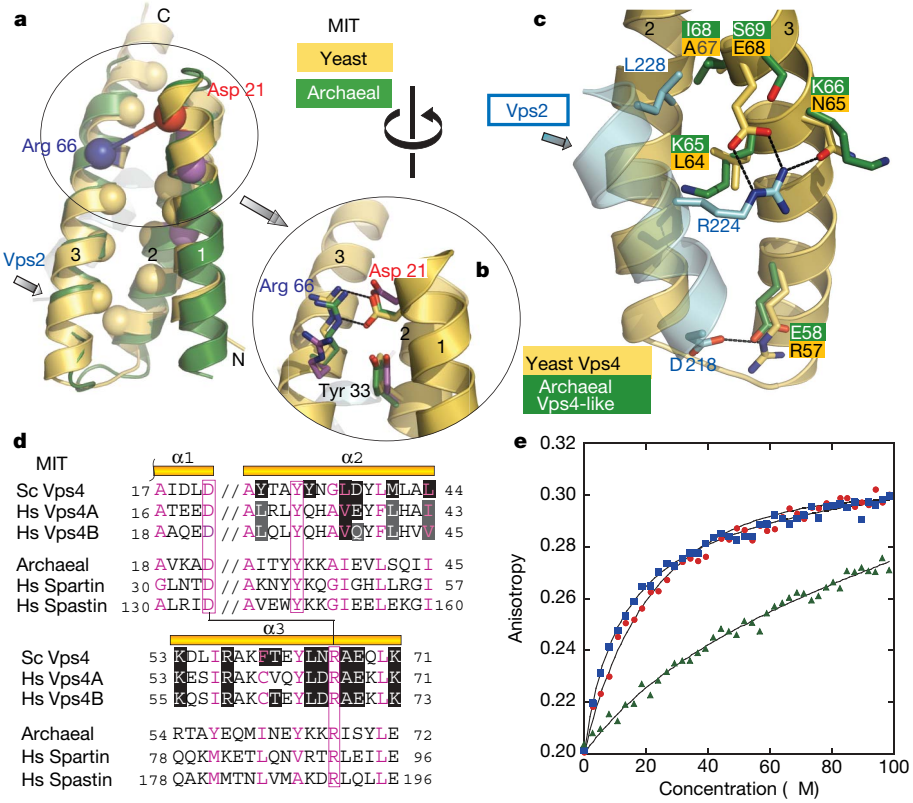

Figure 4 | Conserved features of the MIT domain in ATPases. **a**, Superposition of yeast Vps4 (yellow) and *S. solfataricus* (green) MIT domains. Yellow spheres mark conserved core hydrophobic residues and magenta spheres mark small (Gly or Ala) residues. **b**, Close-up of conserved salt link (including spartin MIT domain (magenta); PDB 2DL1). **c**, Residues in the Vps4–Vps2 interface that differ from the archaeal Vps4-like ATPase. **d**, Selected MIT domains, with conserved residues shown in magenta and ESCRT-III interface residues blackened. Sc, yeast; Hs, human. **e**, Binding of archaeal ESCRT-III-like (SSO0910) C-terminal constructs (titrants) to the archaeal Vps4-like MIT domain, determined by fluorescence anisotropy. Residues 164–207 (blue squares) are both necessary and sufficient (K_d 15 μM). Residues 164–259 (red circles) bind with similar affinity (K_d 20 μM), whereas residues 211–259 (green triangles) do not interact ($K_d > 100$ μM).

this (Fig. 4e). As expected, given the divergence of the archaeal MIT surface (Fig. 4c, d), archaeal ESCRT-III does not bind yeast Vps4 MIT domain (data not shown). The function of the ATPase and ESCRT-III-like components in *S. solfataricus* and other Crenarchaeota is unknown, but Archaea have no endomembrane system, suggesting that ESCRT-III and Vps4 may be relics of a more ancient function common to both Eukaryota and Archaea.

As observed for target binding by other AAA ATPases[30], the isolated Vps4 MIT domain has only a modest affinity for its target ESCRT-III. However, a dodecameric Vps4 should bind an ESCRT-III lattice with a great avidity. Both Vps4-interacting ESCRT-III-related subunits, Vps2 and Did2, are required for efficient vacuolar sorting[6]. Furthermore, the N terminus of Did2 interacts directly with the Vps2–Vps24 subcomplex. Association of the two MIT domain interactors in the same ESCRT-III lattice could enhance the avidity for Vps4. On the ATP hydrolysis-induced transition of Vps4 to a monomer, the low affinity of a single MIT domain for ESCRT-III would facilitate the rapid dissociation of Vps4 from ESCRTs.

The ESCRT-III lattice triggers its own disassembly. It recruits monomeric or dimeric Vps4 to membranes on which the multimeric ESCRT-III lattice facilitates the assembly of the active Vps4 oligomer. Once the ATPase rings have assembled, ATP hydrolysis would lead to the disassembly of both the ATPase rings and the ESCRT-III lattice (Supplementary Fig. 1).

METHODS SUMMARY

The ESCRT-III constructs and the yeast MIT domain were cloned and expressed in *Escherichia coli* with an N-terminal glutathione *S*-transferase (GST) tag. The proteins were purified on glutathione-Sepharose and cleaved with TEV protease, which leaves a four-residue extension, GSHM, at the N terminus. The archaeal MIT domain was expressed with an N-terminal His_6 tag and purified by metal-affinity chromatography. All proteins were further purified by gel filtration. For the crystal structure determinations, Se-Met-substituted proteins were expressed in B834(DE3) cells. For binding measurements, the MIT domains were expressed with a fluorescein bis-arsenical helix binder tag (FlAsH) and fluorescently labelled with Lumio Green (Invitrogen). Binding affinities were determined by titrating protein into a cuvette containing FlAsH-tagged MIT domain and by measuring either a change in fluorescence intensity (yeast MIT domain) or anisotropy (archaeal MIT domain). To enhance the anisotropy change produced by the binding of peptide to the archaeal MIT domain, peptides were titrated as GST fusions.

For the complex of the Vps4 MIT domain with Vps2, the two components were purified separately and mixed for crystallization. The crystal structures were determined by using multiple-wavelength anomalous diffraction (MAD) methods with synchrotron data collected from crystals at 100 K.

Full Methods and any associated references are available in the online version of the paper at www.nature.com/nature.

Received 28 May; accepted 15 August 2007.

1. Ogura, T. & Wilkinson, A. J. AAA+ superfamily ATPases: common structure—diverse function. *Genes Cells* **6**, 575–597 (2001).
2. Slagsvold, T., Pattni, K., Malerod, L. & Stenmark, H. Endosomal and non-endosomal functions of ESCRT proteins. *Trends Cell Biol.* **16**, 317–326 (2006).
3. Williams, R. L. & Urbe, S. The emerging shape of the ESCRT machinery. *Nature Rev. Mol. Cell Biol.* **8**, 355–368 (2007).
4. Bieniasz, P. D. Late budding domains and host proteins in enveloped virus release. *Virology* **344**, 55–63 (2006).
5. Carlton, J. G. & Martin-Serrano, J. Parallels between cytokinesis and retroviral budding: a role for the ESCRT machinery. *Science* **316**, 1908–1912 (2007).
6. Nickerson, D. P., West, M. & Odorizzi, G. Did2 coordinates Vps4-mediated dissociation of ESCRT-III from endosomes. *J. Cell Biol.* **175**, 715–720 (2006).

7. Babst, M., Wendland, B., Estepa, E. J. & Emr, S. D. The Vps4p AAA ATPase regulates membrane association of a Vps protein complex required for normal endosome function. *EMBO J.* **17,** 2982–2993 (1998).
8. Howard, T. L., Stauffer, D. R., Degnin, C. R. & Hollenberg, S. M. CHMP1 functions as a member of a newly defined family of vesicle trafficking proteins. *J. Cell Sci.* **114,** 2395–2404 (2001).
9. Amerik, A., Nowak, J., Swaminathan, S. & Hochstrasser, M. The Doa4 deubiquitinating enzyme is functionally linked to the vacuolar protein-sorting and endocytic pathways. *Mol. Biol. Cell* **11,** 3365–3380 (2000).
10. Tsang, H. T. *et al.* A systematic analysis of human CHMP protein interactions: Additional MIT domain-containing proteins bind to multiple components of the human ESCRT III complex. *Genomics* **88,** 333–346 (2006).
11. von Schwedler, U. K. *et al.* The protein network of HIV budding. *Cell* **114,** 701–713 (2003).
12. Bowers, K. *et al.* Protein–protein interactions of ESCRT complexes in the yeast *Saccharomyces cerevisiae*. *Traffic* **5,** 194–210 (2004).
13. Martin-Serrano, J., Yarovoy, A., Perez-Caballero, D. & Bieniasz, P. D. Divergent retroviral late-budding domains recruit vacuolar protein sorting factors by using alternative adaptor proteins. *Proc. Natl Acad. Sci. USA* **100,** 12414–12419 (2003).
14. Vajjhala, P. R., Catchpoole, E., Nguyen, C. H., Kistler, C. & Munn, A. L. Vps4 regulates a subset of protein interactions at the multivesicular endosome. *FEBS J.* **274,** 1894–1907 (2007).
15. Scott, A. *et al.* Structure and ESCRT-III protein interactions of the MIT domain of human VPS4A. *Proc. Natl Acad. Sci. USA* **102,** 13813–13818 (2005).
16. Bishop, N. & Woodman, P. ATPase-defective mammalian VPS4 localizes to aberrant endosomes and impairs cholesterol trafficking. *Mol. Biol. Cell* **11,** 227–239 (2000).
17. Scott, A. *et al.* Structural and mechanistic studies of VPS4 proteins. *EMBO J.* **24,** 3658–3669 (2005).
18. Babst, M., Katzmann, D. J., Estepa-Sabal, E. J., Meerloo, T. & Emr, S. D. ESCRT-III: an endosome-associated heterooligomeric protein complex required for MVB sorting. *Dev. Cell* **3,** 271–282 (2002).
19. Muziol, T. *et al.* Structural basis for budding by the ESCRT-III factor CHMP3. *Dev. Cell* **10,** 821–830 (2006).
20. Lin, Y., Kimpler, L. A., Naismith, T. V., Lauer, J. M. & Hanson, P. I. Interaction of the mammalian endosomal sorting complex required for transport (ESCRT) III protein hSnf7-1 with itself, membranes, and the AAA+ ATPase SKD1. *J. Biol. Chem.* **280,** 12799–12809 (2005).
21. Zamborlini, A. *et al.* Release of autoinhibition converts ESCRT-III components into potent inhibitors of HIV-1 budding. *Proc. Natl Acad. Sci. USA* **103,** 19140–19145 (2006).
22. Agromayor, M. & Martin-Serrano, J. Interaction of AMSH with ESCRT-III and deubiquitination of endosomal cargo. *J. Biol. Chem.* **281,** 23083–23091 (2006).
23. McCullough, J. *et al.* Activation of the endosome-associated ubiquitin isopeptidase AMSH by STAM, a component of the multivesicular body-sorting machinery. *Curr. Biol.* **16,** 160–165 (2006).
24. Whitley, P. *et al.* Identification of mammalian Vps24p as an effector of phosphatidylinositol 3,5-bisphosphate-dependent endosome compartmentalization. *J. Biol. Chem.* **278,** 38786–38795 (2003).
25. Yorikawa, C. *et al.* Human CHMP6, a myristoylated ESCRT-III protein, interacts directly with an ESCRT-II component EAP20 and regulates endosomal cargo sorting. *Biochem. J.* **387,** 17–26 (2005).
26. Takasu, H. *et al.* Structural characterization of the MIT domain from human Vps4b. *Biochem. Biophys. Res. Commun.* **334,** 460–465 (2005).
27. Scheuring, S. *et al.* Mammalian cells express two VPS4 proteins both of which are involved in intracellular protein trafficking. *J. Mol. Biol.* **312,** 469–480 (2001).
28. Reid, E. *et al.* The hereditary spastic paraplegia protein spastin interacts with the ESCRT-III complex-associated endosomal protein CHMP1B. *Hum. Mol. Genet.* **14,** 19–38 (2005).
29. Field, M. C., Gabernet-Castello, C. & Dacks, J. B. in *Origins and Evolution of Eukaryotic Endomembranes and Cytoskeleton* (ed. Jékely, G.) 84–96 (Eurekah/Landes Bioscience Press, Austin, TX, 2007).
30. Hartman, J. J. & Vale, R. D. Microtubule disassembly by ATP-dependent oligomerization of the AAA enzyme katanin. *Science* **286,** 782–785 (1999).

Supplementary Information is linked to the online version of the paper at www.nature.com/nature. A summary figure is also included.

Acknowledgements We thank M. Babu for advice on the archaeal genome analysis. We acknowledge the European Synchrotron Radiation Facility for provision of synchrotron radiation facilities and we thank G. Cioci, D. Flot, I. Leiros and G. Leonard for assistance in using beamlines ID23-2 and ID23-1. T.O. was supported by a JSPS fellowship and S.S. by a fellowship from the Howard Hughes Medical Institute. This research was supported by the Howard Hughes Medical Institute (S.D.E.) and the Medical Research Council (R.L.W.).

Author Information The atomic coordinates of the yeast Vps2–Vps4 MIT-domain complex and the *S. solfataricus* MIT domain are deposited in the Protein Data Bank under accession numbers 2V6X and 2V6Y, respectively. Reprints and permissions information is available at www.nature.com/reprints. Correspondence and requests for materials should be addressed to R.L.W. (rlw@mrc-lmb.cam.ac.uk).

METHODS

Protein cloning, expression and purification. Yeast Vps4 MIT domain (residues 1–82), full-length yeast Vps4 (residues 1–437), Vps2 C terminus (residues 183–232), Snf7 C terminus (residues 177–240), Vps20 C terminus (residues 170–221), Vps24 C terminus (residues 180–224), Did2 C terminus (residues 171–204) and Vps60 C terminus (residues 183–229) were cloned with an N-terminal GST tag in the pOPTG vector and expressed in C41(DE3)RIPL cells. Full-length Vps2 used for pull-down experiments was expressed with an N-terminal MAHHHHHH tag. For crystallography, the Se-Met-substituted protein was expressed in a B834(DE3) methionine auxotroph. Cells were lysed in buffer A (20 mM Tris-HCl, pH 8.0 at 4 °C, 100 mM NaCl and 1 mM dithiothreitol (DTT)) and incubated with glutathione-Sepharose 4B (GE Healthcare) for 1 h. After being washed, the GST fusion protein was digested with TEV protease (100:1 w/w) at 4 °C for 12 h on the resin. The TEV-eluted protein was further purified by gel filtration on a Superdex 75 16/60 column in buffer B (Tris-HCl, pH 7.4 at 20 °C, 100 mM NaCl and 1 mM DTT). Vps2 mutants were also cloned with an N-terminal GST tag in the pOPTG vector, expressed in C41(DE3) cells and purified with the same methods as for the Vps2 C terminus (residues 183–232). *Sulfolobus solfataricus* ESCRT-III-like protein (SSO0910) constructs (residues 164–259, 164–207 and 211–259) were amplified by polymerase chain reaction (PCR) from genomic DNA, expressed and purified similarly to Vps2 constructs except that the GST tag was not cleaved. All constructs were verified by sequencing.

The His_6FlAsH-tagged yeast Vps4 MIT domain was expressed by using the pOPTHF vector in C41(DE3)RIPL cells. Cells were lysed in buffer C (20 mM Tris-HCl pH 8.0, 20 mM imidazole, 100 mM NaCl and 2 mM 2-mercaptoethanol). The protein was purified on a 5-ml His-Trap-FF column equilibrated with the same buffer. The column was washed in the same buffer with 0.1% Triton X-100 and the protein was eluted with an imidazole gradient. Subsequent purification was conducted on a HiTrap-Q column (GE Healthcare) in buffer D (20 mM Tris-HCl, pH 8.5 at 20 °C, 1 mM DTT) and a NaCl gradient. The eluted protein was digested with TEV protease (100:1 w/w) at 4 °C for 12 h to remove the His_6 tag, then purified by gel filtration on a Superdex 75 16/60 column in buffer E (Tris-HCl, pH 7.4 at 20 °C, 100 mM NaCl and 1 mM tris(2-carboxyethyl)phosphine-HCl (TCEP)). FlAsH-tagged Vps4 MIT domain (10 nmol) was labelled with 10 nmol of Lumio Green detection reagent (Invitrogen) in buffer E (containing 5 mM 2-mercaptoethanol) in a final reaction volume of 1 ml for 2 h at 4 °C. The sample was dialysed overnight against buffer E (containing 5 mM 2-mercaptoethanol) at 4 °C with a 3.5-kDa Slide-A-Lyzer membrane (Pierce). The His_6FlAsH-tagged full-length Vps2 (residues 1–232) and the archaeal MIT domain were also expressed by using the pOPTHF vector and purified similarly to the His_6FlAsH-tagged Vps4 MIT domain except that the His_6-tag was not cleaved with TEV.

The MIT domain from the N terminus of the *S. solfataricus* Vps4-like ATPase (accession number SSO0909) was PCR amplified from genomic DNA and cloned into a pOPTH vector, encoding an N-terminal MAHHHHHH tag. The Se-Met-substituted protein was expressed in B834(DE3) cells at 37 °C for 3 h after induction with isopropyl β-D-thiogalactoside at a D_{600} of 1.0. The protein was purified by Ni-affinity chromatography, anion exchange and gel filtration (20 mM Tris-HCl pH 8, 100 mM NaCl, 2 mM DTT).

Yeast plasmid construction and yeast strains. Yeast plasmids and strains are described in Supplementary Methods.

Microscopy. Living cells expressing the GFP–CPS chimaera were harvested at a D_{600} of 0.4–0.7, labelled with FM4-64 for vacuolar membrane staining and resuspended in medium for visualization. Visualization of cells was performed on a fluorescence microscope (Axiovert S1002TV; Carl Zeiss MicroImaging) equipped with fluorescein isothiocyanate and rhodamine filters, captured with a digital camera (CH350 CCD; Photometrix), and deconvolved with Delta Vision software (Applied Precision). Results presented were based on observations of more than 120 cells.

Crystallization. The LMB nanolitre crystallization robotic facility was used for a broad initial screen of 1,440 crystallization conditions. Optimal crystals for the complex of the yeast Vps4 MIT domain (residues 1–82) with Vps2 C terminus (residues 183–232) (both cleaved from GST fusions) were obtained at 17 °C by vapour diffusion from a protein solution at 28 mg ml^{-1} containing a 1:1.7 molar ratio of MIT:Vps2 and a reservoir solution containing 2.0 M $(NH_4)_2SO_4$ and 0.1 M HEPES (pH 7.0). Crystals were cryoprotected by adding glycerol to a final concentration of 25% and frozen by immersion in liquid nitrogen.

The *S. solfataricus* MIT domain was crystallized in sitting drops by vapour diffusion by mixing 2 μl of reservoir solution (0.6 M ammonium tartrate and 2% PEG4K) with 1 μl of protein solution (9 mg ml^{-1} in gel filtration buffer). Crystals appeared within three days after incubation at 17 °C. For data collection, a crystal in a MicroMount loop (MiTeGen) was placed on a Proteros free-mounting system, and all excess liquid was then removed from the loop with a piece of filter paper. The loop was then rapidly immersed in liquid nitrogen.

Crystallographic structure determination. Data for the Vps2–Vps4 complex were collected at 100 K on ESRF beamlines ID23-1 and ID23-2 with the use of two crystals (see Supplementary Methods). The figure-of-merit for the Se-Met MAD refinement after AutoSHARP was 0.3 and after Density Modification (DM) was 0.92. The Ramachandran plot had 96.4% of residues in the core regions and none disallowed. Data collection and refinement statistics are given in Supplementary Tables 1 and 2.

Se-MET MAD data for the archaeal MIT domain were collected at 100 K on ESRF beamline ID23-1. The figure-of-merit after AutoSHARP was 0.44 and after DM was 0.85. The Ramachandran plot had 94.9% of residues in the core regions and none disallowed.

Fluorescence titration binding assay. Analyte protein was titrated into a cuvette containing 15 nM Vps4 MIT domain, 33 nM full-length Vps2 or 20 nM archaeal MIT domain N-terminally labelled with Lumio Green (FlAsH-MIT and FlAsH-Vps2) in 1.1 ml of binding buffer (20 mM Tris-HCl, pH 7.4 at 20 °C, 100 mM NaCl and 5 mM 2-mercaptoethanol). Fluorescence was measured with a Perkin-Elmer LS-55 spectrophotometer with an excitation wavelength of 490 nm and an emission wavelength of 530 nm. Excitation and emission slits were either 10 nm or 15 nm and 20 nm, respectively. A 1.0–1.5-mM protein analyte was titrated into a cuvette with a MicroLab 500 titrator (Hamilton). The K_d values were calculated from a direct fitting of the titration data to a single-site model. At least two independent experiments were conducted to determine K_d values.